

Singlet–triplet physics and shell filling in carbon nanotube double quantum dots

H. INGERSLEV JØRGENSEN^{1,2*}, K. GROVE-RASMUSSEN², K.-Y. WANG¹, A. M. BLACKBURN¹, K. FLENSBERG², P. E. LINDELOF² AND D. A. WILLIAMS¹

¹Hitachi Cambridge Laboratory, Hitachi Europe Ltd, Cambridge CB3 0HE, UK

²Niels Bohr Institute, Nano-Science Center, University of Copenhagen, Universitetsparken 5, DK-2100 Copenhagen Ø, Denmark

*e-mail: hij@fys.ku.dk

Published online: 15 June 2008; doi:10.1038/nphys987

An artificial two-atomic molecule, also called a double quantum dot (DQD), is an ideal system for exploring few-electron physics^{1,2}. Interactions between just two electrons have been explored in such systems using the singlet and triplet states as the two states in a quantum two-level system^{3–7}. An alternative and attractive material for studying spin-based two-level systems is the carbon nanotube (CNT), because it is expected to have a very long spin coherence time⁵. Here, we show that the CNT DQD^{8–13} has a clear shell structure of either four or eight electrons. We show that few-electron physics can be explored in these shells and we find that the singlet and triplet states are present in the four-electron shells. Furthermore, we observe inelastic cotunnelling via the singlet and triplet states, which we use to probe the splitting between the singlet and triplet, in good agreement with theory.

To explore the physics of few electrons, control of the number of interacting electrons is needed. This control has so far been obtained using semiconducting materials operated close to the bandgap edge^{3–7,14–18}. In this letter, we show that nanotubes can be used to obtain the same kind of control. Owing to a robust shell structure, spin states can be identified in nanotube quantum dots even for high filling numbers^{19–23}. Here, we show a CNT DQD exhibiting shell structure in both quantum dots¹⁰, which enables us to identify spin states of the DQD. This is in contrast to DQDs fabricated in other materials^{3–7,14,15}, where the spin states in practice have to be determined by finding the absolute number of electrons, that is, the device has to be operated close to the bandgap edge.

The device analysed here, schematically shown in Fig. 1a, comprises a CNT contacted by titanium source and drain electrodes and gated with three top-gate electrodes, G1, CG (centre gate) and G2, made of aluminium oxide and titanium^{10–12}. The device has two strongly coupled quantum dots in series, as confirmed by the observation of the so-called honeycomb pattern in plots of current (I_{sd}) versus voltage applied to G1 (V_{G1}) and G2 (V_{G2}) (Figs 1b and 2a)¹. The two dots have roughly equal charging energies and level spacings (see below), from which we infer that the tunnelling barrier between the two dots is located under, or close to the centre gate. As the room-temperature gate dependence of the device is metallic, the tunnelling barrier is most likely due to a defect under the centre gate formed during electron beam lithography. We have seen similar barriers in other devices fabricated by the same method. The number of electrons in dot 1 and dot 2 can be controlled by tuning V_{G1} and V_{G2} , respectively. In the middle of each hexagon

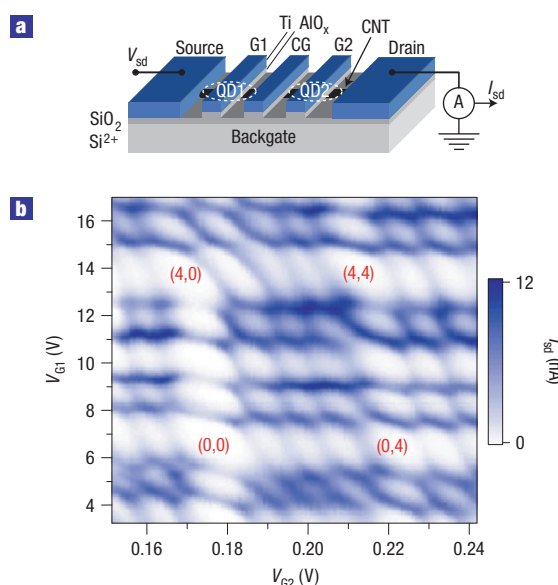


Figure 1 Shell filling of a CNT DQD. **a**, Schematic diagram of the device consisting of a CNT contacted by titanium source and drain electrodes and gated with three top-gate electrodes, G1, CG (centre gate) and G2. Two quantum dots (QD1, QD2) are formed in series, one under G1 and one under G2. **b**, Surface plot of current (I_{sd}) at constant bias ($V_{sd} = 0.5$ mV) as a function of voltage applied to G1 (V_{G1}) and G2 (V_{G2}) with $V_{CG} = 0$ V and at $T = 0.35$ K. Red numbers (N, M) are shell occupation numbers for one eight-electron (DQD) shell. Two further eight-electron shells were observed in connection with this shell, one below, and one to the right.

(white areas in Figs 1b and 2a), a fixed number of electrons are localized in each dot, and electron transport is suppressed by Coulomb blockade. Along the entire edge of the hexagons (blue lines), sequential tunnelling is allowed through molecular states formed in the DQD, indicating a strong coupling between the two dots. The height (width) of the hexagons corresponds to the energy required to add an extra electron in dot 1 (dot 2). In Fig. 1b, the width and height of the hexagons alternate in size in a regular pattern. The four hexagons marked with red

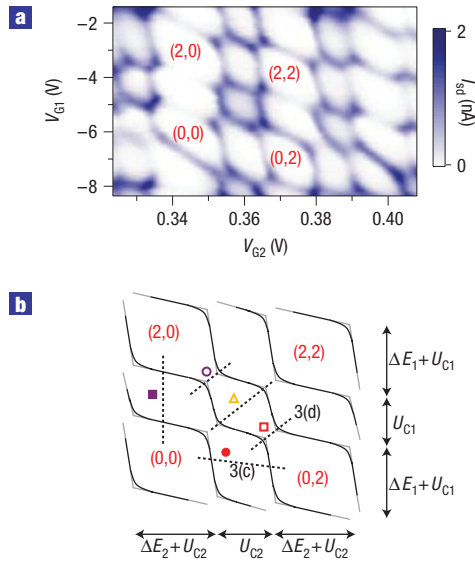


Figure 2 Four-electron DQD-shell structure. **a**, Surface plot of current (I_{sd}) at constant bias ($V_{sd} = 0.2$ mV) as a function of voltage applied to G1 (V_{G1}) and G2 (V_{G2}) with $V_{CG} = 0$ V and at $T = 0.35$ K. The numbers (N, M) are shell occupation numbers for one four-electron shell. The charging energies and level spacings for the two dots are $U_{C1} \sim 3$ meV and $U_{C2} \sim 3.5$ meV, and $\Delta E_1 \sim 1.2$ meV and $\Delta E_2 \sim 1.5$ meV, respectively (see text). **b**, Black lines: schematic honeycomb diagram for a four-electron shell with strong tunnel coupling, and a small cross capacitance. Grey lines: same honeycomb diagram with negligible tunnel coupling. Dashed lines indicate where the line traces in Fig. 3 are measured.

numbers are distinctively larger than the other hexagons, with three smaller hexagons in between, indicating that each dot has four-fold degenerate levels due to spin and orbital degeneracy^{19–21}. An eight-electron shell structure of the DQD can therefore be identified in this plot. Shell occupation numbers (N, M), where N (M) is the level occupation number in dot 1 (dot 2), are written on the honeycomb diagram.

The honeycomb diagram in Fig. 2a is measured for the same device but in another gate region where a new pattern in the sizes of the hexagons is observed. The hexagons alternate in size between large and small owing to only spin degeneracy of the energy levels in each dot^{19,22}, yielding a four-electron shell structure of the DQD. The charging energies (U_{C1}, U_{C2}) and level spacings ($\Delta E_1, \Delta E_2$) for the two dots can be extracted from the honeycomb pattern as schematically shown in Fig. 2b. The gate coupling of G1 (G2) to dot 1 (dot 2) is found from bias spectroscopy plots (not shown), and we find $U_{C1} \sim 3$ meV and $\Delta E_1 \sim 1.2$ meV for dot 1, and $U_{C2} \sim 3.5$ meV and $\Delta E_2 \sim 1.5$ meV for dot 2. As charging energy and level spacing are almost identical for the two dots, we deduce that the two dots are roughly equal in size. We have observed both four-electron and eight-electron shell structures in two different devices.

Herein, we will focus on a four-electron shell with level spacings and charging energies similar to the four-electron shell shown in Fig. 2a, except $\Delta E_1 \sim 1.9$ meV. We show in the following that singlet and triplet states are formed in this four-electron shell. The singlet ground state between region (1,1) and (0,2) is in general a bonding state of the local singlet ($S(02)$, both electrons in dot 2) and the non-local singlet ($S(11)$, one electron in each dot):

$$S_B = \alpha S(11) + \beta S(02).$$

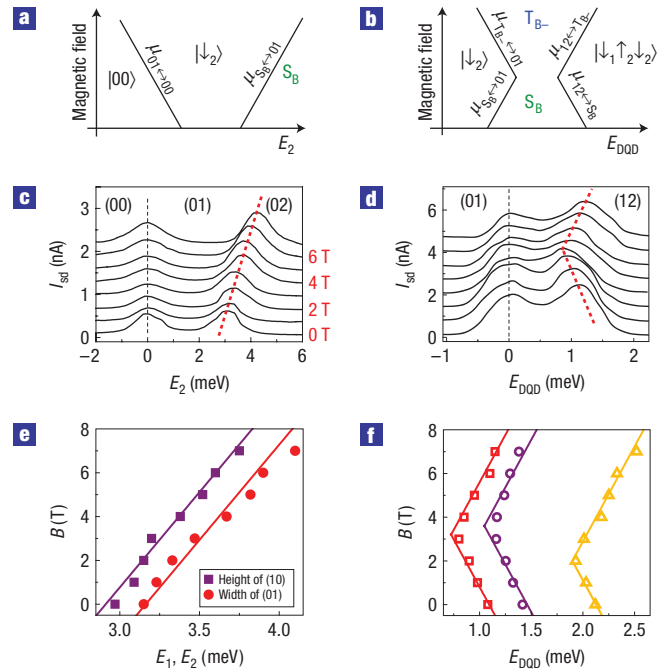


Figure 3 Singlet and triplet states in a four-electron shell. **a–d**, Theoretical (**a, b**) and measured (**c, d**) magnetic field dependence of the chemical potentials, where $E_{D00} = 1/2(E_1 + E_2)$. In **a, c**, the four-electron shell is filled from zero electrons ($|00\rangle$), to one spin-down electron in dot 2 ($|\downarrow_2\rangle$), to a singlet (S_B). In **b, d**, the four-electron shell is filled from a spin-down electron in dot 2 ($|\downarrow_2\rangle$), to either a singlet (S_B) or a triplet (T_{B-}) (see text), to a three-particle state ($|\downarrow_1 \uparrow_2 \downarrow_2\rangle$). The line traces in **c, d** are extracted from honeycomb diagrams measured at $B = 0, 1, 2, \dots, 7$ T, where B is perpendicular to the nanotube. Each line in **c, d** is offset 0.3 nA and 0.7 nA, respectively, for clarity, and the left-most peak is centred at zero. **e**, Width of hexagon (01) (circles) (extracted from **c**) and height of hexagon (10) (squares) versus B . **f**, Size of hexagon (11) versus B at three values of detuning, as indicated in Fig. 2b. Squares are extracted from **d**. The solid lines in **e, f** are the Zeeman energy $g\mu_B B$, with $g = 2$ for nanotubes.

The detuning ($\varepsilon = E_2 - E_1$)-dependent parameters α and β determine the weight of each state, and E_1 and E_2 are the electrostatic potentials in dot 1 and dot 2, respectively. Similarly for the triplets

$$T_{B-} = \alpha' T_{-(11)} + \beta' T_{-(02)},$$

$$T_{B0} = \alpha' T_0(11) + \beta' T_0(02),$$

$$T_{B+} = \alpha' T_{+(11)} + \beta' T_{+(02)},$$

where $-, 0, +$ denotes the spin magnetic moment in the z direction, $S_z = -1, 0, +1$. In the following, we will show the existence of the singlet and triplet states on the basis of magnetic field spectroscopy on the four-electron shell.

In Fig. 3c, we analyse the magnetic field dependence of the width of hexagon (0,1), which involves 0, 1, and 2 electrons in dot 2. The chemical potential for these two Coulomb peaks is given by²: $\mu_{01 \leftrightarrow 00} \propto -(1/2)g\mu_B B$ and $\mu_{S_B \leftrightarrow 01} \propto +(1/2)g\mu_B B$, where $\mu_{01 \leftrightarrow 00}$ is the chemical potential for adding an electron to charge state (01) given no electron in the DQD shell, and $\mu_{S_B \leftrightarrow 01}$ is the chemical potential for adding an electron in state S_B given one electron charge state (01). These two Coulomb peaks are therefore

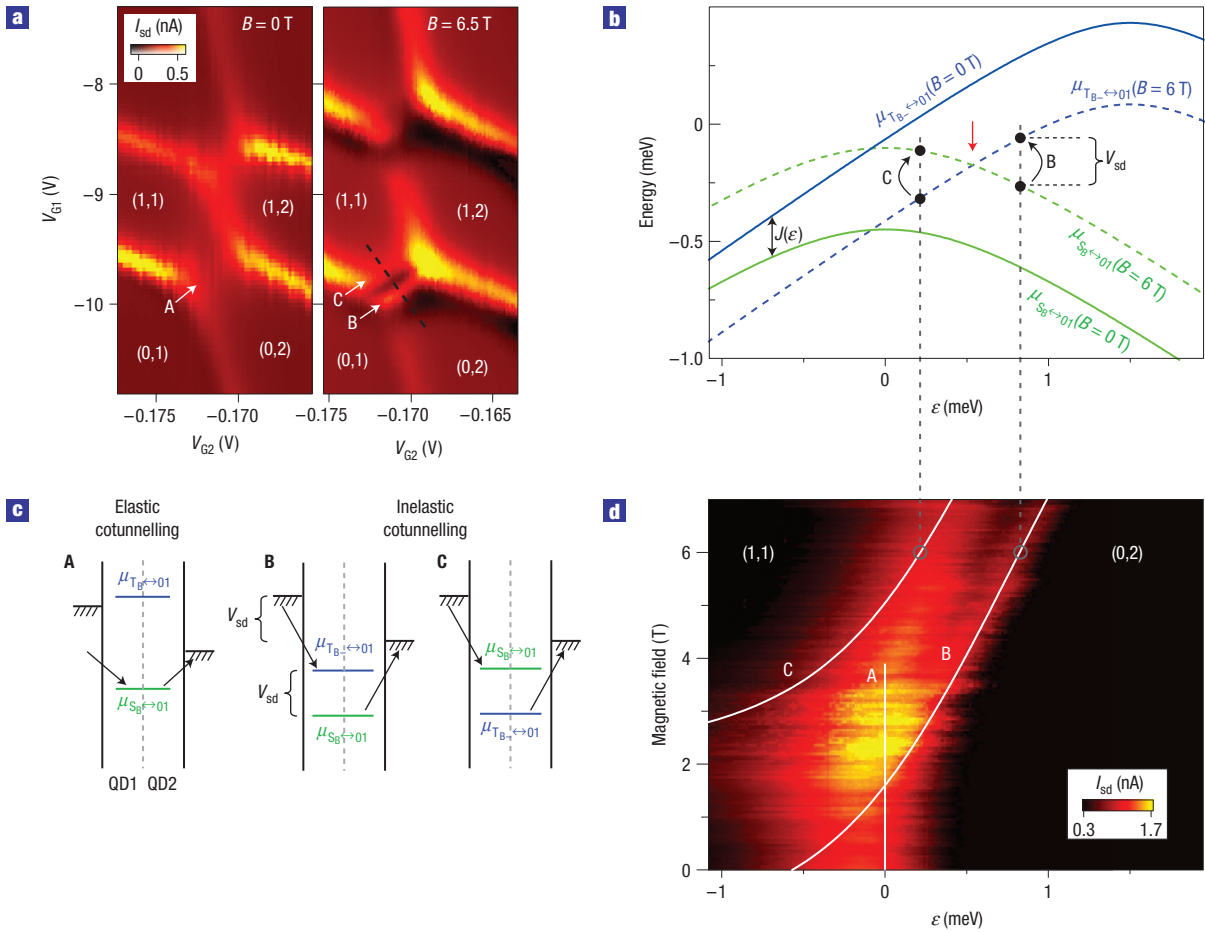


Figure 4 Singlet–triplet splitting probed by inelastic cotunnelling. **a**, Small section of the honeycomb diagram analysed in Fig. 3 with $V_{sd} = 50 \mu\text{V}$ at $B = 0$ T (left) and $B = 6.5$ T (right). The numbers (N, M) indicate electron occupation of the four-electron shell. **b**, Chemical potentials for the singlet bonding ($\mu_{S_{B-} \leftrightarrow 01}$) and triplet bonding ($\mu_{T_{B-} \leftrightarrow 01}$) with $B = 0$ T (solid green and blue lines) and with $B = 6$ T (dashed green and blue lines) calculated using equations (1) and (2). Onset of inelastic cotunnelling that excites electrons from singlet to triplet (black arrow marked B) and from triplet to singlet (black arrow marked C) occurs when the separation between $\mu_{S_{B-} \leftrightarrow 01}$ and $\mu_{T_{B-} \leftrightarrow 01}$ is equal to eV_{sd} . **c**, Schematic transport diagrams for elastic cotunnelling (A) and inelastic cotunnelling (B and C). **d**, Surface plot of current (I_{sd}) at $V_{sd} = 0.2$ mV versus magnetic field (B), and detuning (ϵ) along the black dashed line in **a**. Onset of inelastic cotunnelling occurs along the white lines marked B and C, calculated using equation (3) with $t = 0.32$ meV, $\Delta E_2 = 1.5$ meV, $V_{sd} = 0.2$ mV and $g = 2$. Dashed grey lines indicate where the two inelastic cotunnelling processes shown in **b** occur.

expected to separate by $g\mu_B B$, as shown in Fig. 3a. The height of hexagon (1,0) is similarly expected to separate by $g\mu_B B$. The measured height of hexagon (1,0) and width of hexagon (0,1) versus magnetic field are in good agreement with theory, as shown in Fig. 3e.

We now analyse the size of hexagon (1,1), which involves 1, 2 and 3 electrons in the DQD shell. We show that by applying a magnetic field the two-electron ground state can be changed from S_B to T_{B-} , which is used to estimate the exchange energy (J) (energy separation between S_B and T_{B0}). Transport at the first Coulomb peak in Fig. 3d is through different chemical potentials at low and high magnetic field, given by $\mu_{S_{B-} \leftrightarrow 01} \propto + (1/2)g\mu_B B$ at low magnetic field ($g\mu_B B < J$), and $\mu_{T_{B-} \leftrightarrow 01} \propto - (1/2)g\mu_B B$ at high magnetic field ($g\mu_B B > J$). Similarly, transport at the second Coulomb peak in Fig. 3d is through $\mu_{12 \leftrightarrow S_B} \propto - (1/2)g\mu_B B$ at low magnetic field ($g\mu_B B < J$) and through $\mu_{12 \leftrightarrow T_{B-}} \propto + (1/2)g\mu_B B$ at high magnetic field ($g\mu_B B > J$)². Therefore, for increasing magnetic field, the gap between the two Coulomb peaks at the (1,1) to (0,2) anticrossing decreases when S_B is ground state, and

increases when T_{B-} is ground state, as schematically shown in Fig. 3b. The measurement in Fig. 3d is in good agreement with Fig. 3b, with the bend (change of ground state from singlet to triplet) occurring at $B \sim 3.2$ T, that is, an exchange energy of $J \sim 0.37$ meV. The magnetic field dependence of the size of hexagon (1,1) at three constant values of detuning (Fig. 3f) shows that the exchange energy is minimum at the centre of hexagon (1,1), with the bend occurring at $B \sim 2$ T, that is, $J \sim 0.23$ meV. The exchange energy can also be estimated from the tunnel coupling strength (t). We estimate $t \sim 0.32$ meV from the curvature of the hexagons at the (1,1) to (0,2) anticrossing (see the Supplementary Information)¹¹. This estimate of t yields a consistent estimate of the exchange energy $J \sim 4(t\sqrt{2})^2/U_{C1} \sim 0.27$ meV (ref. 2) for large detuning (at $\epsilon = U_{C1}$, the centre of hexagon (11)), and $J \sim t\sqrt{2} \sim 0.45$ meV at the anticrossing (see the Supplementary Information).

The anticrossing between (1,1) and (0,2) is analysed in Fig. 4. We find that transport is governed by elastic and inelastic cotunnelling via S_B and T_{B-} . The chemical potential for adding an electron to S_B and T_{B-} with $E_1 + E_2 = 0$, that is, along the

black dashed line in Fig. 4a, is given by (see the Supplementary Information):

$$\mu_{S_B \leftrightarrow 01}(\varepsilon, B) = -\frac{1}{2}\sqrt{(2t\sqrt{2})^2 + \varepsilon^2} + \frac{1}{2}g\mu_B B \quad (1)$$

$$\mu_{T_{B-} \leftrightarrow 01}(\varepsilon, B) = -\frac{1}{2}\left(\sqrt{(2t)^2 + (\varepsilon - \Delta E_2)^2} - \Delta E_2\right) - \frac{1}{2}g\mu_B B. \quad (2)$$

We plot equations (1) and (2) in Fig. 4b with $B = 0$ T (solid green and blue lines) and with $B = 6$ T (dashed green and blue lines). We see that S_B is ground state for $B = 0$ T, and that the two chemical potentials cross at elevated magnetic field, indicated with a red arrow.

At low magnetic field, one broad peak in conductance versus detuning between (1,1) and (0,2) is seen (Fig. 4a, white arrow marked A). This conductance peak is due to elastic cotunnelling via S_B , schematically shown in Fig. 4c (marked A). As elastic cotunnelling via S_B involves both $S(11)$ and $S(02)$, which have equal weight at $\varepsilon = 0$, the elastic cotunnelling peak is centred around $\varepsilon = 0$. At high magnetic field, the elastic cotunnelling via S_B becomes suppressed because the ground state at $\varepsilon = 0$ changes from S_B to T_{B-} . Figure 4d shows a surface plot of I_{sd} versus ε and B along the black dashed line in Fig. 4a. The white vertical line marked A is the expected position of the elastic cotunnelling.

At high magnetic field, we observe two narrow peaks, marked B and C in Fig. 4a. These two narrow peaks are due to the onset of inelastic cotunnelling via S_B and T_{B-} , schematically shown in Fig. 4c marked B and C. Onset of inelastic cotunnelling via S_B and T_{B-} occurs when the energy separation between their chemical potentials becomes equal to the applied bias:

$$eV_{sd} = \pm(\mu_{S_B \leftrightarrow 01}(\varepsilon, B) - \mu_{T_{B-} \leftrightarrow 01}(\varepsilon, B)). \quad (3)$$

We have calculated the onset of inelastic cotunnelling in (ε, B) -space from these two conditions and plotted it as white lines marked B and C in Fig. 4d. Note that no fitting parameters are used in Fig. 4d; the parameters used, $t = 0.32$ meV, $\Delta E_2 = 1.5$ meV, were found in the analysis above.

METHODS

FABRICATION AND MEASUREMENT SET-UP

The devices are made on a highly doped silicon substrate with a top layer of silicon dioxide. The CNTs are grown by chemical vapour deposition from islands of catalyst material and subsequently contacted by 50 nm titanium source and drain electrodes. Next, three narrow top-gate electrodes are fabricated between the source and drain electrodes, consisting of aluminium oxide and titanium¹². A schematic diagram of the device together with the measurement set-up is shown in Fig. 1a. Source–drain voltage (V_{sd}) is applied to the source electrode and the drain electrode is connected through a current-to-voltage amplifier to ground. The three top-gate electrodes are

named G1, CG (centre gate) and G2, starting from the source electrode. For the device reported here, we saw that G1 had a much lower gate coupling than G2 and CG (see Figs 1b and 2a), which we attribute to the G1 electrode being damaged somewhere, weakening its gate coupling. The gate coupling of G1 to dot 1 is $\alpha_{G1} = 2.9$ meV V^{-1} , and the gate coupling of G2 to dot 2 is $\alpha_{G2} = 400$ meV V^{-1} . The centre gate is kept at $V_{CG} = 0$ V for the measurements shown here. All data presented here are measured in a sorption pumped ^3He cryostat at 350 mK.

Received 23 November 2007; accepted 8 May 2008; published 15 June 2008.

References

- van der Wiel, W. G. *et al.* Electron transport through double quantum dots. *Rev. Mod. Phys.* **75**, 1–22 (2002).
- Hanson, R., Kouwenhoven, L. P., Petta, J. R., Tarucha, S. & Vandersypen, L. M. K. Spins in few-electron quantum dots. *Rev. Mod. Phys.* **79**, 1217–1265 (2007).
- Petta, J. R. *et al.* Coherent manipulation of coupled electron spins in semiconductor quantum dots. *Science* **309**, 2180–2184 (2005).
- Koppens, F. H. L. *et al.* Control and detection of singlet–triplet mixing in a random nuclear field. *Science* **309**, 1346–1350 (2005).
- Johnson, A. C. *et al.* Triplet–singlet spin relaxation via nuclei in a double quantum dot. *Nature* **435**, 925–928 (2005).
- Johnson, A. C., Petta, J. R., Marcus, C. M., Hanson, M. P. & Gossard, A. C. Singlet–triplet spin blockade and charge sensing in a few-electron double quantum dot. *Phys. Rev. B* **72**, 165308 (2005).
- Ono, K., Austing, D. G., Tokura, Y. & Tarucha, S. Current rectification by Pauli exclusion in a weakly coupled double quantum dot system. *Science* **297**, 1313–1317 (2002).
- Mason, N., Biercuk, M. J. & Marcus, C. M. Local gate control of a carbon nanotube double quantum dot. *Science* **303**, 655–658 (2004).
- Biercuk, M. J., Garaj, S., Mason, N., Chow, J. M. & Marcus, C. M. Gate-defined quantum dots on carbon nanotubes. *Nano Lett.* **5**, 1267–1271 (2005).
- Sapmaz, S., Meyer, C., Beliczynski, P., Jarillo-Herrero, P. & Kouwenhoven, L. P. Excited state spectroscopy in carbon nanotube double quantum dots. *Nano Lett.* **6**, 1350–1355 (2006).
- Gräber, M. R. *et al.* Molecular states in carbon nanotube double quantum dots. *Phys. Rev. B* **74**, 075427 (2006).
- Jørgensen, H. I., Grove-Rasmussen, K., Hauptmann, J. R. & Lindelof, P. E. Single wall carbon nanotube double quantum dot. *Appl. Phys. Lett.* **89**, 232113 (2006).
- Gräber, M. R., Weiss, M. & Schönenberger, C. Defining and controlling double quantum dots in single-walled carbon nanotubes. *Semicond. Sci. Technol.* **21**, 64–68 (2006).
- Nowack, K. C., Koppens, F. H. L., Nazarov, Y. V. & Vandersypen, L. M. K. Coherent control of a single electron spin with electric fields. *Science* **318**, 1430–1433 (2007).
- Pfund, A., Shorubalko, I., Ensslin, K. & Leturcq, R. Suppression of spin relaxation in an InAs nanowire double quantum dot. *Phys. Rev. Lett.* **99**, 036801 (2007).
- Elzerman, J. M. *et al.* Few-electron quantum dot circuit with integrated charge read out. *Phys. Rev. B* **67**, 161308 (2003).
- Fuhrer, A. *et al.* Few electron double quantum dots in InAs/InP nanowire heterostructures. *Nano Lett.* **7**, 243–246 (2007).
- Hayashi, T., Fujisawa, T., Cheong, H. D., Jeong, Y. H. & Hirayama, Y. Coherent manipulation of electronic states in a double quantum dot. *Phys. Rev. Lett.* **91**, 226804 (2003).
- Cobden, D. H. & Nygård, J. Shell filling in closed single-wall carbon nanotube quantum dots. *Phys. Rev. Lett.* **89**, 046803 (2002).
- Moriyama, S., Fuse, T., Suzuki, M., Aoyagi, Y. & Ishibashi, K. Four-electron shell structures and an interacting two-electron system in carbon-nanotube quantum dots. *Phys. Rev. Lett.* **94**, 186806 (2005).
- Buitelaar, M. R., Bachtold, A., Nussbaumer, T., Iqbal, M. & Schönenberger, C. Multiwall carbon nanotubes as quantum dots. *Phys. Rev. Lett.* **88**, 156801 (2002).
- Moriyama, S., Fuse, T., Aoyagi, Y. & Ishibashi, K. Excitation spectroscopy of two-electron shell structures in carbon nanotube quantum dots in magnetic fields. *Appl. Phys. Lett.* **87**, 073103 (2005).
- Sapmaz, S. *et al.* Electronic excitation spectrum of metallic carbon nanotubes. *Phys. Rev. B* **71**, 153402 (2005).

Supplementary Information accompanies this paper on www.nature.com/naturephysics.

Acknowledgements

We wish to acknowledge the support of the EU FP6 STREP projects ULTRA-1D and CARDEQ, as well as the FP6 IP projects SECOQC and CANAPE. We were also supported by the Danish Research Council, FTP-274-05-0178.

Author information

Reprints and permission information is available online at <http://npg.nature.com/reprintsandpermissions>. Correspondence and requests for materials should be addressed to H.L.J.